JGR Oceans

RESEARCH ARTICLE
10.1029/2021JC018333

Influence of Kelp Forest Biomass on Nearshore Currents

Stephen G. Monismith[1], Maha W. Alnajjar[1], C. Brock Woodson[2], Charles A. Boch[3,4], Arturo Hernandez[5], Leonardo Vazquez-Vera[5,6], Tom W. Bell[7], and Fiorenza Micheli[3,8]

[1]Department of Civil and Environmental Engineering, Stanford University, Stanford, CA, USA, [2]College of Engineering, University of Georgia, Athens, GA, USA, [3]Hopkins Marine Station, Stanford University, Pacific Grove, CA, USA, [4]Monterey Bay Aquarium Research Institute, Moss Landing, CA, USA, [5]Comunidad y Biodiversidad, La Paz, Mexico, [6]The Nature Conservancy, La Paz, Mexico, [7]Department of Applied Ocean Physics and Engineering, Woods Hole Oceanographic Institution, Woods Hole, MA, USA, [8]Stanford Center for Ocean Solutions, Pacific Grove, CA, USA

Abstract As part of a project focused on the coastal fisheries of Isla Natividad, an island on the Pacific coast of Baja California, Mexico, we conducted a 2-1/2 year study of flows at two sites within the island's kelp forests. At one site (Punta Prieta), currents are tidal, whereas at the other site (Morro Prieto), currents are weaker and may be more strongly influenced by wind forcing. Satellite estimates of the biomass of the giant kelp (*Macrocystis pyrifera*) for this period varied between 0 (no kelp) and 3 kg/m^2 (dense kelp forest), including a period in which kelp entirely was absent as a result of the 2014–2015 "Warm Blob" in the Eastern Pacific. During this natural "deforestation experiment", alongshore velocities at both sites when kelp was present were substantially weaker than when kelp was absent, with low-frequency alongshore currents attenuated more than higher frequency ones, behavior that was the same at both sites despite differences in forcing. The attenuation of cross-shore flows by kelp was less than alongshore flows; thus, residence times for water inside the kelp forest, which are primarily determined by cross-shore velocities, were only weakly affected by the presence or absence of kelp. The flow changes we observed in response to changes in kelp density are important to the biogeochemical functioning of the kelp forest in that slower flows imply longer residence times, and, are also ecologically relevant in that reduced tidal excursions may lead to more localized recruitment of planktonic larvae.

Plain Language Summary Observations of flows were made during a two and one half year period when the state of kelp forests in the nearshore of an island off Baja California varied between lush and nonexistent. These measurements are used to show how density of kelp biomass affects currents in the nearshore of the island. Notably, the effects vary with the frequency with which the currents vary, and are much stronger for flows along the coast as opposed to cross-shore flows that control exchange water in the kelp forest with water offshore.

Key Points:

- Time series of nearshore currents at two sites measured over a 30-month period when the local kelp forests were both lush and completely absent allows direct inference of the effects of kelp biomass on local flows
- Alongshore velocities at both sites when kelp was present were much weaker than when kelp was absent, with low-frequency currents attenuated more than higher frequency ones
- Because attenuation of cross-shore flows was less than alongshore flows, residence times for water inside the kelp forest were only weakly affected by the presence or absence of kelp

Supporting Information:

Supporting Information may be found in the online version of this article.

Correspondence to:

S. G. Monismith,
monismith@stanford.edu

Citation:

Monismith, S. G., Alnajjar, M. W., Woodson, C. B., Boch, C. A., Hernandez, A., Vazquez-Vera, L., et al. (2022). Influence of kelp forest biomass on nearshore currents. *Journal of Geophysical Research: Oceans*, *127*, e2021JC018333. https://doi.org/10.1029/2021JC018333

Received 10 DEC 2021
Accepted 15 JUN 2022

Author Contributions:

Conceptualization: Stephen G. Monismith, Maha W. Alnajjar, C. Brock Woodson, Tom W. Bell, Fiorenza Micheli
Data curation: Tom W. Bell
Formal analysis: Stephen G. Monismith, Maha W. Alnajjar
Funding acquisition: Stephen G. Monismith
Investigation: Stephen G. Monismith, Maha W. Alnajjar, C. Brock Woodson, Charles A. Boch, Arturo Hernandez, Leonardo Vazquez-Vera, Tom W. Bell, Fiorenza Micheli

1. Introduction

In coastal regions of the eastern Pacific Ocean, as well as in Australia, Tasmania, and New Zealand, dense stands of giant kelp (*Macrocystis pyrifera*) are common. These kelp forests are hotspots of biodiversity and productivity, providing a suite of critical ecosystem services including coastal protection, carbon sequestration, fisheries, and tourism (Arafeh-Dalmau et al., 2020; McCay et al., 2014). Ecologically relevant flows in these ecosystems are associated with tides, surface wind stresses, and internal and surface waves (see review in Gaylord et al. [2012]). Most notably, while kelp appears to have little effect on incident swell (Elwany et al., 1995), kelp forests can significantly weaken nearshore currents (Gaylord et al., 2007; Jackson & Winant, 1983; Rosman et al., 2007). Such changes can have broad reaching impacts on nutrient delivery, larval supply, and ecosystem function (Gaylord et al., 2012; Wheeler, 1980). For example, Jackson and Winant (1983) reported overall velocity reductions of flows inside a kelp forest in southern California by a factor of 1/3 relative to flows outside, and noted both damping of semidiurnal tidal components and attenuation of incident internal waves. Similarly, for a smaller kelp forest, Gaylord et al. (2007) observed depth-averaged velocities that were 1.5–5 times slower than currents in kelp-free regions (Gaylord et al., 2007).

As part of a larger interdisciplinary study of socio-ecological systems based in nearshore fisheries at Isla Natividad, Baja California, Mexico (Micheli et al., 2012; Woodson et al., 2018), we observed extreme variations in the density (0 to >3 kg m^{-2}) of *Macrocystis pyrifera* due to a multiyear period of temperatures well above long-term

Methodology: Stephen G. Monismith, Maha W. Alnajjar, C. Brock Woodson, Tom W. Bell, Fiorenza Micheli
Project Administration: Stephen G. Monismith, Fiorenza Micheli
Software: Stephen G. Monismith, Tom W. Bell
Supervision: Stephen G. Monismith, Fiorenza Micheli
Validation: Tom W. Bell
Writing – original draft: Stephen G. Monismith, Maha W. Alnajjar
Writing – review & editing: Stephen G. Monismith, Maha W. Alnajjar, C. Brock Woodson, Charles A. Boch, Arturo Hernandez, Leonardo Vazquez-Vera, Tom W. Bell, Fiorenza Micheli

averages. While kelp forest biomass is inherently dynamic, the anomalous warm water conditions observed starting in 2014 led to massive losses of kelp biomass across its range in the NE Pacific (Cavanaugh et al., 2019; Reed et al., 2016). These severe losses in biomass are uncommon on subdecadal scales (Bell et al., 2020). Thus, the complete disappearance of the kelp forest surrounding Isla Natividad observed in 2014 allows for an unprecedented opportunity to quantify the influence of kelp forest state on the flow around a complex coastal system.

In this paper, we use observations made during this natural experiment to assess how kelp biomass variations affect several aspects of flows through the Isla Natividad kelp forests and consider these observations in light of the theory of flow through living roughness like that provided by the kelp. In what follows we describe the observed temporal variations in biomass, currents, surface waves, and temperatures, highlighting differences in physical conditions at the two sites, and at each site as kelp biomass varied. In addition to documenting the dramatic changes in the strength of depth-averaged currents that accompany changes in kelp biomass, we discuss the frequency dependence of attenuation of currents, showing that low-frequency alongshore currents are most strongly affected by kelp drag, behavior that is consistent with unsteady canopy flow theory (Lowe et al., 2005). Strikingly, although flows at the two sites differ in many respects, the overall attenuation of flows by kelp is the same for both sites. Lastly, we also consider how these flow variations affect residence time and alongshore transport, hydrodynamic characteristics that are important to kelp forest biogeochemistry, larvae dispersal, and larval connectivity.

1.1. Theoretical Considerations

While it is well known that flows inside a kelp forest, like flows through other vegetation (Nepf, 2012), are weaker than flows outside the kelp forest, the physics involved is surprisingly complicated, depending on details of the kelp geometry including particularly the surface canopy, which can change with flow (Gaylord et al., 2008; Utter & Denny, 1996), the geometry of the kelp forest as a whole (Rominger & Nepf, 2011), the presence or absence of waves (Rosman et al., 2013), and possible interactions among these factors.

As a starting point, consider the depth-averaged momentum equations assuming that the wave forcing is negligible (e.g., Arzeno et al., 2018; Rominger & Nepf, 2011):

$$\frac{\partial \vec{U}}{\partial t} + \vec{U} \cdot \nabla \vec{U} = -g\nabla\eta - \vec{F}_K - \vec{F}_B \tag{1}$$

Here, $\vec{U}$ is the depth-averaged velocity, η is the free-surface deflection, $\vec{F}_K$ is the drag force associated with kelp, and $\vec{F}_B$ is the drag force associated with bottom stresses. Both $\vec{F}_K$ and $\vec{F}_B$ can depend on waves, and $\vec{F}_K \propto V_K^n$ where the power law dependence is n on the velocity relative to the (moving) kelp, V_K^n can be less than the standard value of 2 (Gaylord et al., 2008; Utter & Denny, 1996). Inside the kelp forest, $g\nabla\eta \simeq -\vec{F}_K$, that is, the local pressure gradient balances drag on the kelp, although, as seen in canopy flows (Lowe et al., 2005), unsteady inertia can remain important such that low-frequency flows are attenuated more by the canopy drag than are high-frequency flows.

This frequency-dependent attenuation by kelp drag can be examined using scaling. In the absence of waves (cf., Lowe et al., 2005):

$$\frac{\partial U}{\partial t} \sim \frac{U}{T} \quad F_K \sim \frac{dhU^2}{(d/s)^2} \Rightarrow \frac{\frac{\partial U}{\partial t}}{F_K} \sim \frac{\frac{1}{T}}{\frac{dhU}{(d/s)^2}} = \left(\frac{d}{sh}\right)^2 \frac{h}{UT} \tag{2}$$

where T is the period of oscillation (e.g., the M2 tidal period), d is the effective kelp sporophyte diameter, equal to the stipe diameter for a single stipe or something larger for multiple stipes on a single individual, h is the local depth, and s is the spacing of the sporophytes. Equation 2, which assumes that the drag coefficient appropriate to individual kelp plants is O(1), implies that drag dominates when the sporophyte spacing is small, the flows are strong, or the time scale of flow variation is long. In this case, all else being equal, alongshore flows, which are typically stronger than cross-shore flows, should be more drag influenced and thus more attenuated by kelp drag.

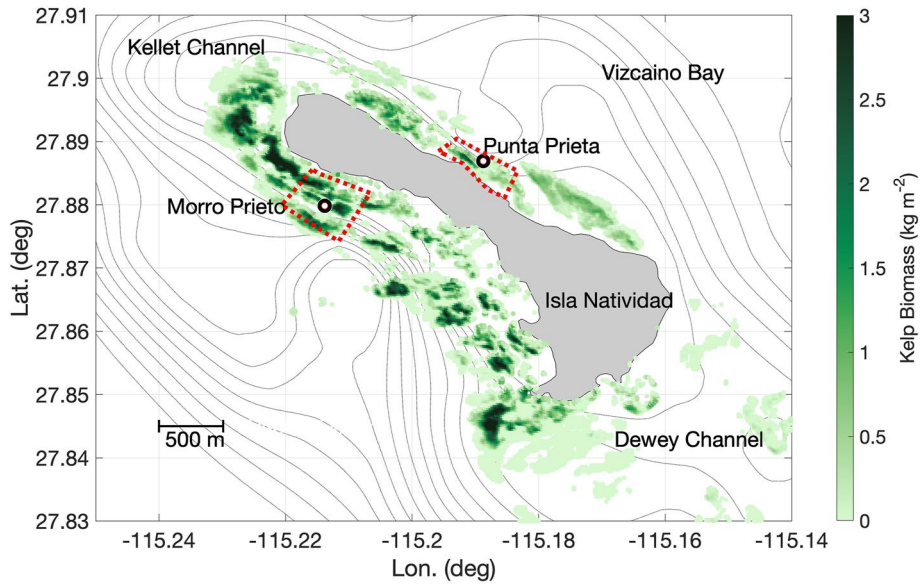

Figure 1. Long-term mooring locations, bathymetry, and the distribution of average satellite-derived kelp biomass during the study period. The dashed red lines show the areas used to estimate the region for which kelp biomass might influence flows at the two moorings.

On the other hand, if the kelp drag is assumed to be wave dominated so that $F_K \propto v_w U$, where v_w is the wave velocity, then

$$\frac{\frac{\partial U}{\partial t}}{F_K} \sim \left(\frac{d}{sh}\right)^2 \frac{h}{v_w T}, \tag{3}$$

so that the extent to which drag dominates is independent of flow strength. In this case, alongshore and cross-shore velocities should be attenuated equally. These two possible models of kelp drag's effect on alongshore and cross-shore flows are examined below.

2. Methods

The data we present come from two long-term moorings deployed in the nearshore waters of Isla Natividad on the Baja California Peninsula (Figure 1) between March 2013 and September 2015. Some aspects of these data are presented elsewhere (Woodson et al., 2018); here, we primarily focus on the velocity measurements. The two mooring locations at Isla Natividad differ in shelf width, slope, exposure to oceanic water, tidal current magnitude, and extent of kelp coverage, each representing distinct but common kelp forest settings across the region. Strong, tidally forced channels over the wide shelf connecting Vizcaíno Bay to the Pacific Ocean characterize Punta Prieta (hereafter PP). In contrast, Morro Prieto (hereafter MP), on the southwest side of the island, is characterized by active upwelling and weak tidal currents (Alnajjar, 2019; Dawson, 1952). Initially, the instrument set was deployed (or redeployed) and recovered on roughly 3-month intervals, later this was extended to 6 months. The result is a set of 6 deployment periods over a period of 2-1/2 years. Because the same instruments were used throughout this period, breaks between deployments were 1–4 days long.

These moorings included bottom-mounted 1 MHz Nortek Acoustic Doppler Profilers (ADPs) and Seabird 37 CTDOs, as well as thermistor chains made up of 3 SBE56 thermistor loggers. Table 1 gives details of the instrument configurations for the PP and MP moorings and references each deployment by location and number, for example, PP3 is the third deployment at Punta Prieta (3/7/13 to 7/2/13). ADP current profiles with 0.5 m resolution were recorded on 5, 10, or 30 min intervals depending on the deployment; these we will refer to as instantaneous velocities. Heights listed below are presented in meters above bed (mab). The moorings themselves were located in sand patches in the middle of nearshore kelp stands. Typical distances from the mooring to nearby kelp were 20 m (PP) and 10 m (MP). We do not have salinity and water column temperature measurements at MP from

Table 1
Instruments and Sampling Details

Period	Dates	Mean vel.[a,b]	Waves[b]	Thermistor chain[c]	CTDO
1 (PP1/MP1)	3/7/13 to 7/2/13	10 min/1 min 0.5 m bins	No	Both: 1,6,11 mab	Both: 10 min
2 (PP2/MP2)	7/4/13 to 9/9/13	10 min/1 min 0.5 m bins	1 hr/1,024@1 Hz 1 m wave bin	Both: 1,6,11 mab	Both: 10 min
3 (PP3/MP3)	9/13/13 to 3/29/14	5 min/30 s 0.5 m bins	1 hr/1,024@1 Hz 2 m wave bin	Both: 1,6,11 mab	Both: 10 min
4 (PP4/MP4)	3/31/14 to 9/10/14	10 min/1 min 0.5 m bins	1 hr/1,024@1 Hz 2 m wave bin	PP: 1,6,11 mab MP: no	PP: 10 min MP: no
5 (PP5/MP5)	9/12/14 to 2/20/15	10 min/1 min 0.5 m bins	1 hr/1,024@1 Hz 2 m wave bin	Both: 1,6,11 mab	Both: 10 min
6 (PP6/MP7)	3/16/15 to 9/11/15	30 min/1 min 0.5 m bins	No	Both: 1,6,11 mab	Both: 10 min

[a]Sampling: Interval between profiles/averaging period for each burst. [b]Sampling: Interval between wave burst/wave burst sampling; Velocity measurements made in bin size shown centered at 0.4 m + (1/2) × (wave bin size). [c]Sampling: 0.5 Hz—data later converted to 10-min averages.

March to September 2014 because the CTDO and thermistors were lost sometime in late August/early September when several hurricanes were present off the coast of Baja California.

Depth-averaged velocities were rotated to alongshore and cross-shore directions by maximizing variance in the alongshore direction (Emery & Thomson, 2004). For the tidally dominated PP mooring, this was done once for the set of 6 deployments taken as a whole. Because of internal compass issues with the ADP at MP, this rotation was done separately for each deployment. Currents and tidal elevations for each of the 6 deployments at both sites were harmonically analyzed using the Matlab™ function *t_tide* (Pawlowicsz et al., 2002).

To quantify changes in flow with kelp biomass, we computed several tidally averaged quantities. We used the Godin moving average filter (Godin, 1972) to estimate time varying root mean square (RMS) values of depth-averaged velocities and other properties, for example, for depth-averaged velocities:

$$V_{\mathrm{rms}} = \left\{F\left(V^2\right)\right\}^{1/2} \tag{4}$$

where F is the Godin filter and V is the depth-averaged alongshore velocity. Given that the Godin filter comprises a sequence of 3 moving averages, it is a variant of a moving average filter described by Bendat and Piersol (2000) as being suitable for computing RMS values of nonstationary signals, albeit one that is well suited for tides.

Flow variability was also quantified using frequency spectra. These were calculated using the Matlab™ function *pwelch*, which implements Welch's FFT-based method for spectra estimation (Emery & Thomson, 2004). While data segment and FFT length varied depending on the data being analyzed, in all cases we used a Hamming window that was half the length of the FFT. In what is shown below, the spectral resolution of the time-varying spectra was not sufficient to separate out different diurnal and semidiurnal band harmonics, and so peaks at these frequencies (1 cpd and 0.5 cpd) likely represent the combination of multiple constituents.

Because surface waves can be important, near-bottom wave velocities and pressures were measured as 1,024 sample bursts once per hour for deployments 2 through 5. As with the mean velocities, RMS wave velocities for each burst were estimated by rotation of the coordinate axes to principal axes for each burst and then computing the burst-averaged RMS value of the instantaneous major axis velocity, v_w. Pressure data were converted to free-surface elevation variations using the frequency and depth-dependent transfer function given by linear wave theory (Dean & Dalrymple, 1991). For each burst, these free surface elevations were then used to compute using spectral moments, average wave period, T_a, and significant wave height, H_s, as described in Dean and Dalrymple (1991). Using linear wave theory, pressure spectra were also used to calculate wave-induced velocities.

The PP velocity data were used to estimate residence time, T_r, defined as the length of time water particles spend in a given region of space (Lucas & Deleersnijder, 2020). Estimates of T_r were computed as follows: For each time step, we released an imaginary particle starting in the center of the kelp forest and used velocities near the bottom and near the surface to calculate subsequent displacements, and thus the time the particle first leaves the kelp forest, that is, for cross-shore flows, the time to go one half the width of the forest (125 m) from its starting point, a time which we define as our residence time estimate. For the alongshore flows, we made a similar calculation, albeit using the half length of the entire kelp forest (1,000 m) on the eastern side of the island as the distance which must be traversed to exit the kelp forest. Given that this procedure can be done for every time at which the ADP measured velocities, what results are distributions of residence times. Note that this approach assumes that the water column is well mixed, an approximation that seems appropriate to describe the general behavior of the flow.

The PP velocity data were also used to calculate a related quantity associated with transport, the tidal excursion, $\zeta(t)$, that is, the horizontal displacement of water particles due to tidal motions. To compute $\zeta(t)$, the tidal velocity, computed by subtracting the tidally filtered velocity from the instantaneous velocity, is integrated in time:

$$\zeta(t) = \int_0^t \{V - F(V)\}\, dt. \tag{5}$$

This was computed separately for each deployment; what is presented below is the RMS value of ζ, a quantity that is independent of the limits of integration in Equation 5.

For purposes of comparison of wind forcing at Morro Prieto, NCEP Reanalysis data for wind speeds were provided by NOAA/OAR/ESRL PSL, Boulder, Colorado, USA, from their website https://psl.noaa.gov/data/gridded/data.ncep.reanalysis.surface.html. Wind velocities at 10 m above the surface for the NCEP grid point closest to Island Natividad were converted to shear velocities using a wind drag coefficient of 1.3×10^{-3}.

Lastly, estimates of kelp biomass at Isla Natividad were obtained using Landsat 7 and 8 (see Bell et al., 2020). The highest temporal resolution possible for this data is 8 days, provided no local cloud cover interferes with the satellite measurements (Bell et al., 2015). The spatial resolution is 30 × 30 m. Since satellite measurements can only capture canopies reaching the water surface, the biomass data are limited to estimates based on the surface canopy biomass. In this analysis, kelp biomass for each of the two sites was estimated by computing the average biomass in each of the boxes shown in Figure 1. The length of these boxes (~600 m) was chosen to correspond approximately to average tidal excursions at each site and the widths to the cross-shore extents of the kelp forest at each site. Experimentation with different size boxes, including ones that extended over the entire length of each side of the island did not substantially change the results. Nonetheless, it is important to note that the region of hydrodynamic influence of the spatially varying density of kelp sporophytes remains an open question.

3. Results

In this section, we present data showing background temperature variations and wave climate; these data provide a basis for understanding the changes in kelp biomass observed throughout our study. This is followed by presentation of the current data, including the harmonic decomposition of currents measured at PP, where tides dominate, and the dependence of current strength on kelp biomass for both sites.

3.1. Long-Term Temperature Variability at Morro Prieto and Punta Prieta

During the spring, warming of the nearshore waters of Isla Natividad is limited by upwelling events that can at times cause decreases in temperatures of up to 5°C along with significant decreases in dissolved oxygen (DO) concentrations (Woodson et al., 2018). Temperatures, and consequently DO concentrations, are generally lower at MP than at PP (Woodson et al., 2018). The different thermal environments of the two sites can be seen in Figures 2a and 2b, power spectra of bottom temperatures as functions of time and frequency for the two sites. Diurnal and semidiurnal variability of temperature at both sites was seasonal, with temperatures being much more variable from April through September than it was for the other 6 months. Subtidal temperature fluctuations, presumably due to upwelling, represent a much larger fraction of the total temperature variance at MP,

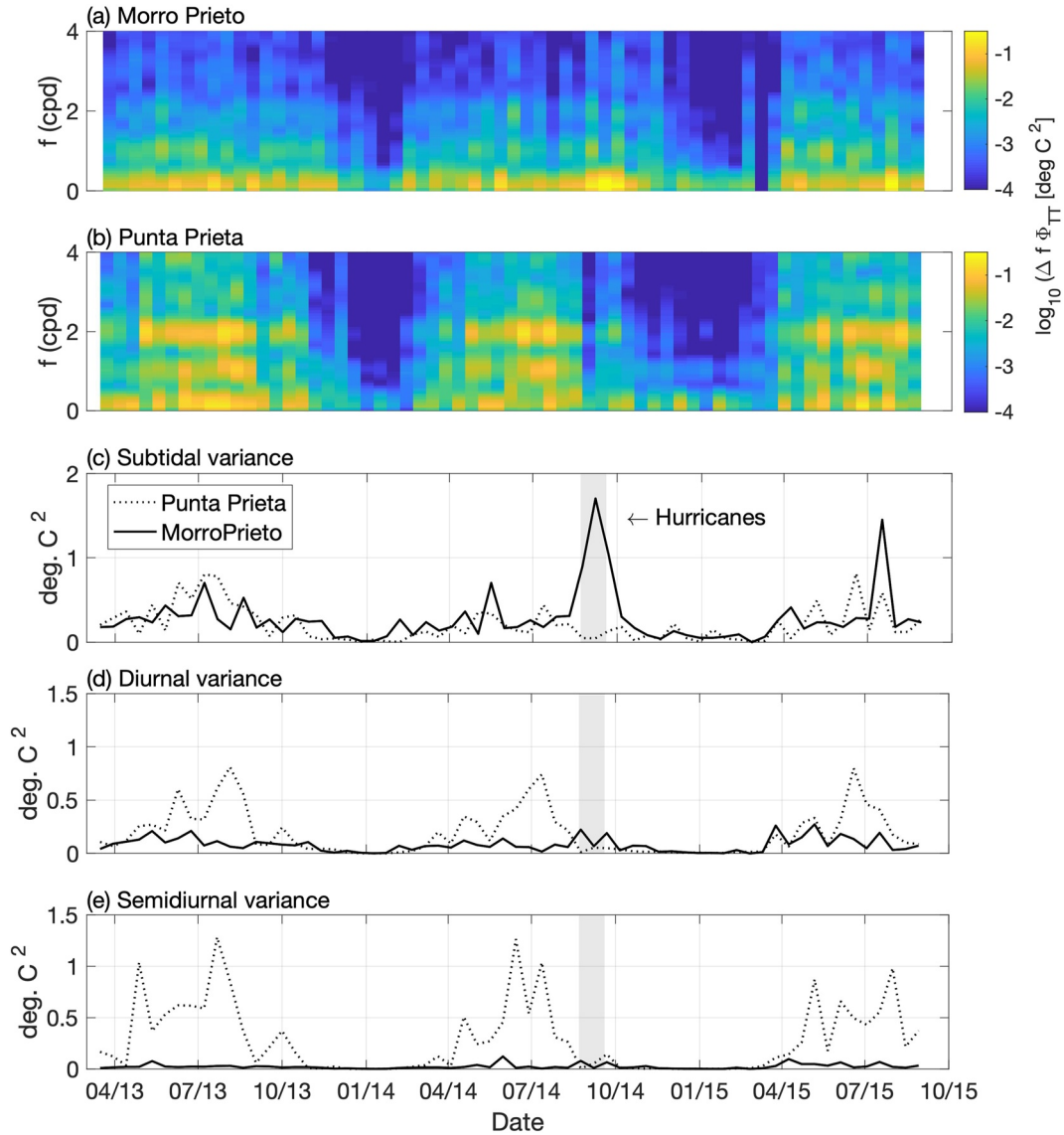

Figure 2. Power spectra as functions of time and frequency, f, at: (a) Morro Prieto and (b) Punta Prieta. Variation in time of bottom temperature variance for: (c) subtidal frequencies ($f < 0.7$ cpd); (d) diurnal frequencies ($0.7 < f < 1.4$ cpd); and (e) semidiurnal frequencies ($1.7 < f < 2.3$ cpd). In this figure and in subsequent figures involving spectra, power spectral densities are multiplied by the FFT resolution, Δf, so that the quantity shown has units of variance. The time series in panels (c–e) were computed by integration of spectra over the specified frequency ranges. The gray shaded region on each panel in this figure and on Figures 3, 4, and 13 mark the period in which three hurricanes may have affected Isla Natividad.

the open ocean side of the island. Nonetheless, aside from two events associated with hurricanes (Hurricanes Marie, Norbert, and Odile in 2014 and Hurricane Dolores in 2015), subtidal temperature variability at the two sites was quite similar (Figure 2c). In contrast, the differences in diurnal and semidiurnal band variances from April to September between the two sites are striking (Figures 2d and 2e): bottom temperatures at PP are far more variable at tidal frequencies than are bottom temperatures at MP. Given that the water column depths at the two sites are similar (13 m at PP vs. 15 m at MP), diurnal temperature changes due to surface heating and cooling at the two sites should be similar; thus, the large difference in diurnal variability must be due to tidal advection and internal waves. Semidiurnal temperature variability is not associated with surface heating and cooling. Moreover, examination of the temperature records at PP show that semidiurnal temperature variations are much stronger near the bottom than near the surface, and so must be associated with internal waves, as reported (e.g.,) by Walter et al. (2014) for a kelp forest in Monterey Bay, central California, USA.

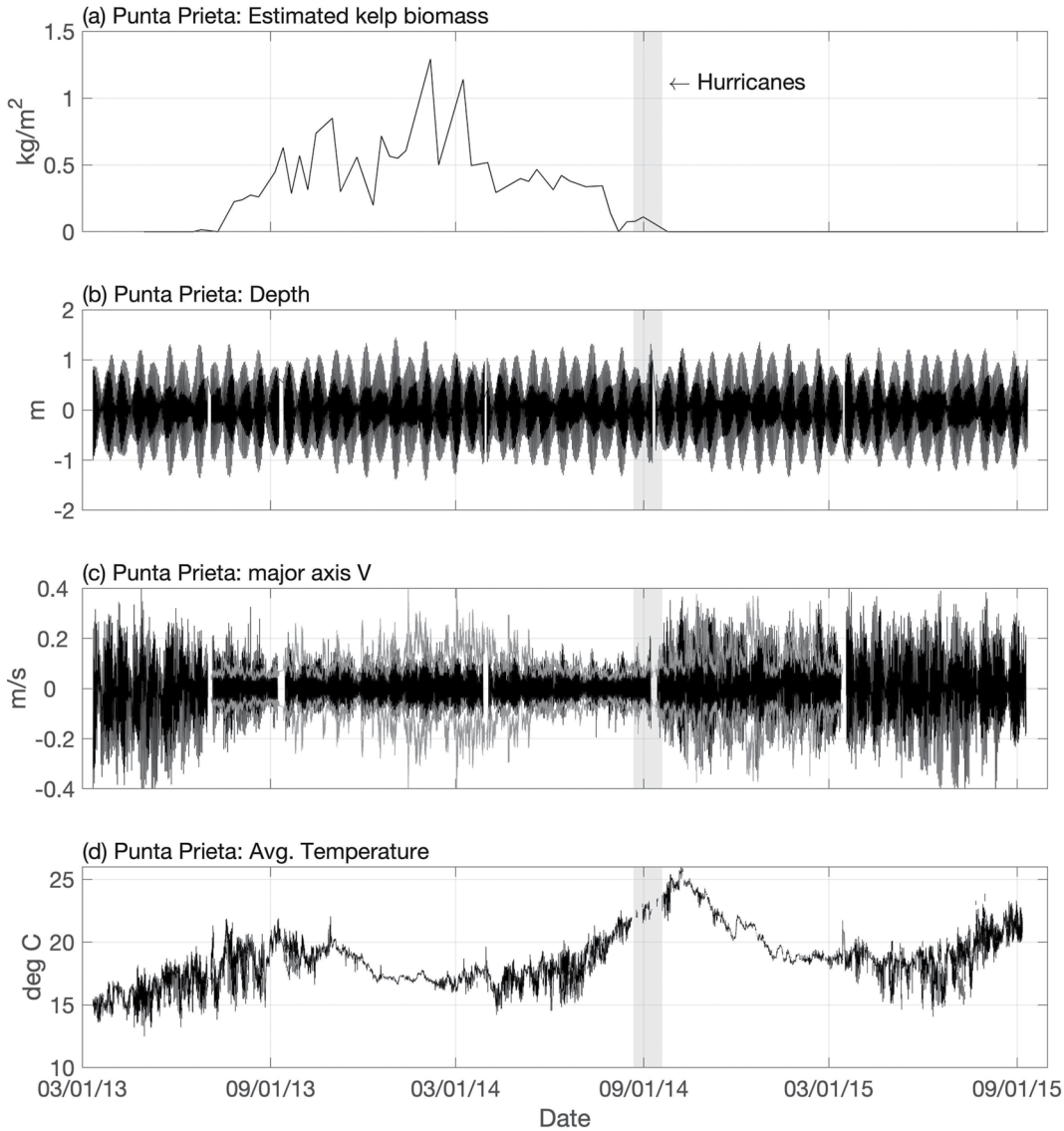

Figure 3. Kelp biomass and flows at Punta Prieta: (a) Satellite-derived kelp biomass estimate; (b) Depth linearly detrended for each deployment; (c) Depth-averaged longshore velocity (—) and ± root mean square near-bottom wave velocity (—); (d) Depth-averaged temperature. The gray shaded region on each panel in this figure and on Figure 4 marks the period in which three hurricanes may have affected Isla Natividad.

3.2. The 2014–2015 Eastern Pacific Warm Blob and the Loss of Kelp Biomass

A key feature of our observations is the unusual warming above 20°C recorded in 2014, with summer to fall transition temperatures at the two sites reaching 25°C by the beginning of October (Figures 3 and 4). These data reflect the general prolonged warming event in the Eastern Pacific between late 2013 and early 2016, an event generally known as the "Warm Blob" (Cavole et al., 2016). During the late summer/early fall of 2014, there was a near complete die-off of the kelp forests through the region, including at Isla Natividad (Figure 5). Additionally, three hurricanes, Marie, Norbert, and Odile, passed near Isla Natividad in late August/early September 2014, likely enhancing the complete removal of kelp from our field sites. Of these, it appears that the first, Marie (22 August–2 September 2014), may have been the most damaging to the Natividad kelp forests in that, as recorded by the satellite, a substantial part of the loss of kelp took place between 15 and 31 August. Significant wave heights at MP during Marie were in excess of 4 m and near-bottom RMS wave velocities reached 0.7 m/s on the morning of 26 August, a value that is much larger than typical RMS wave velocities of ca. 0.2 m/s at MP (Figure S1 in Supporting Information S1). Near-surface velocities calculated spectrally (Dean & Dalrymple, 1991) were likely

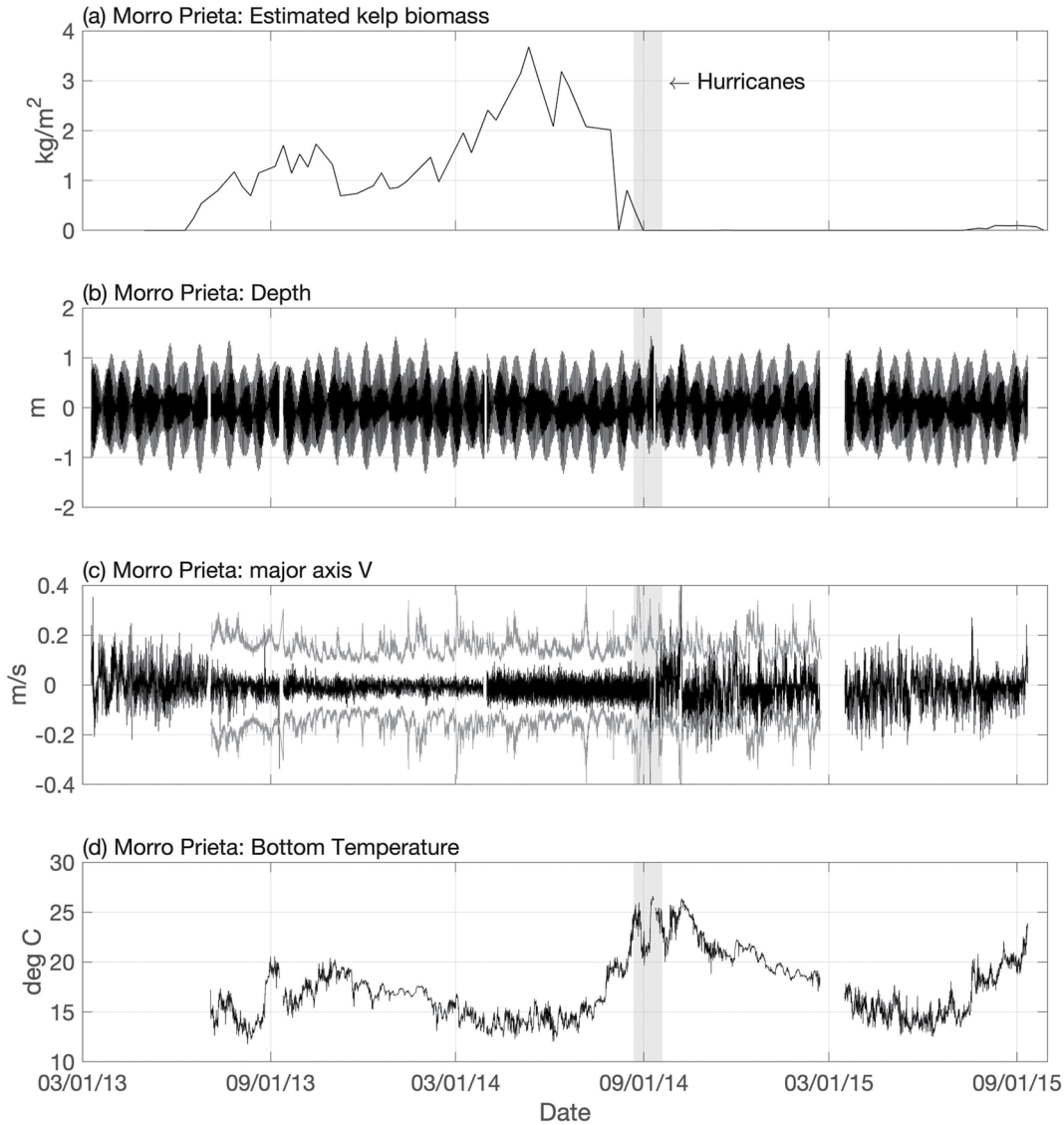

Figure 4. Kelp biomass and flows at Morro Prieto: (a) Satellite-derived kelp biomass estimate; (b) Depth linearly detrended for each deployment; (c) Depth-averaged longshore velocity (—) and ± root mean square near-bottom wave velocity (—); (d) Bottom temperature. Note that in (c), the scale has been limited to ±0.4 m/s, whereas the peak root mean square velocity on 26 August 2014 was 0.7 m/s.

in excess of 1 m/s. Assuming a quadratic drag law, these high velocities mean that the imposed instantaneous drag on kelp plants could have been a factor of 10 larger during the high-wave period associated with Marie than would typically be seen at MP, while the very large height of the waves would also imply enhanced vertical stretching of the kelp plants. Both of these effects are likely to have led to enhanced breaking of kelp stipes (Utter & Denny, 1996), and hence loss of kelp. Nonetheless, comparing Figure 5a (4 June) to Figure 5f (15 August), it is apparent that there was significant loss of kelp prior to Hurricane Marie, as well later to hurricanes Norbert (2–11 September) and Odile (10–19 September). In effect, it appears that the late-summer hurricanes may have delivered the "*coup-de-grace*" to the already damaged Natividad kelp forest.

3.3. Observations of Currents With and Without Kelp

The effect of variability in kelp biomass on flows at both sites can be seen in Figures 3c and 4c. Harmonic decomposition of the depth-averaged alongshore currents at PP show that tidal dynamics drive 70%–80% of the velocity

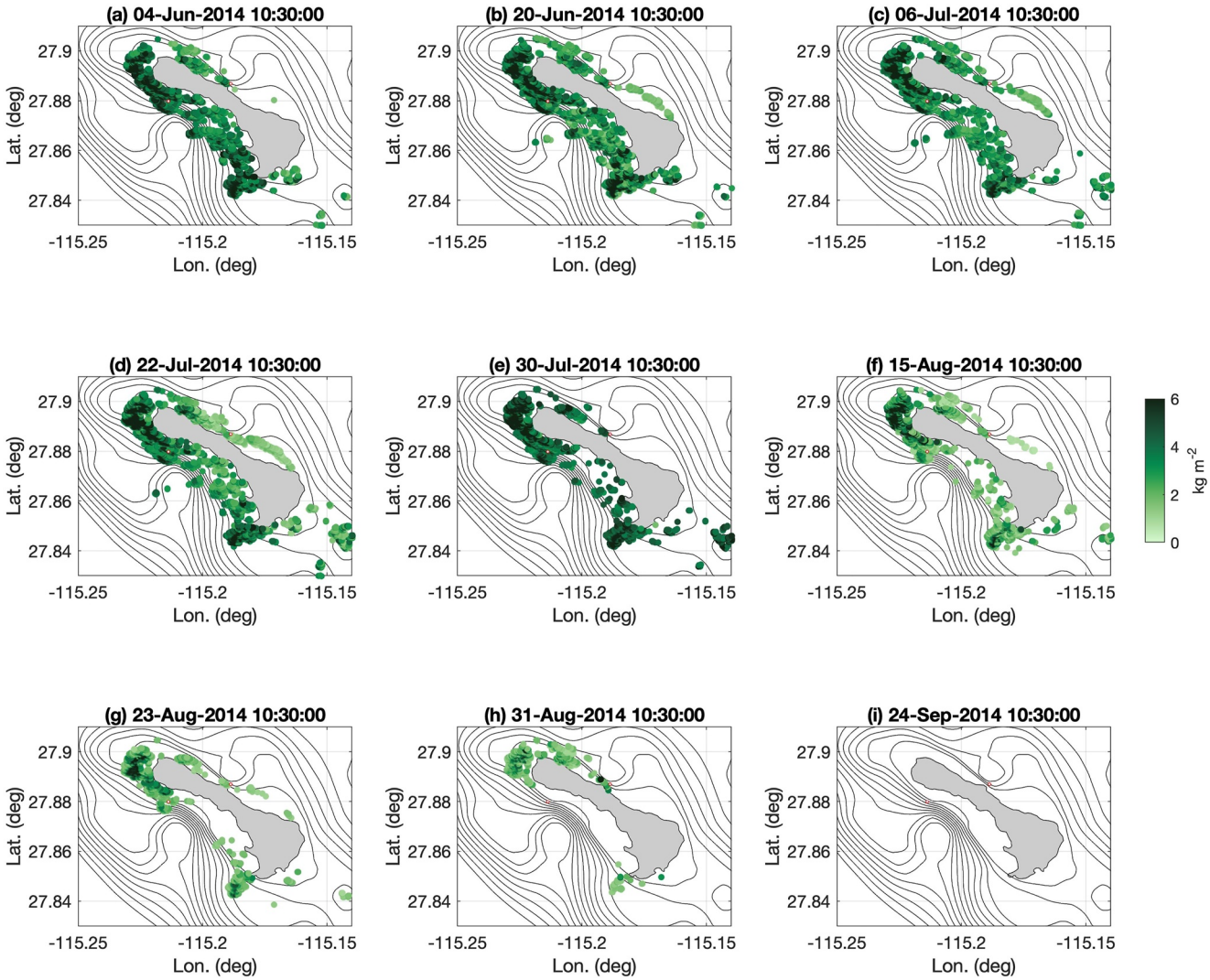

Figure 5. Variation of the satellite-derived kelp biomass distribution near Isla Natividad throughout the summer and early fall of 2014. The red dots mark the locations of the two moorings.

variance (Table S1 in Supporting Information S1). Presumably, this is because these tidal currents are caused by draining and filling of Vizcaíno Bay by flows past the eastern side of Isla Natividad through the Dewey Channel (Figure 1). When kelp biomass is high (up to 1.2 kg/m^2—Figure 3a), these currents are dramatically weaker (Figure 3c) than they are when the kelp is absent. This effect is also reflected in the behavior of the two principal constituents, M2 and K1, estimated separately for each deployment: the M2 velocity amplitude varies by a factor of roughly 3 whereas the K1 velocity amplitude varies by more than a factor of 4, although there is little variation in the tidal elevation amplitudes for either constituent (Table S1 in Supporting Information S1; Figure 3b). The increase in velocity variability observed in September 2014 is likely associated with the complete loss of kelp by September 2014, and, as shown below, the fact that the effects of kelp reach their maximum strength for relatively low values of kelp biomass density. Thus, the difference in flow behavior between August and September shows that flows through sparse kelp forests are different than are flows in the absence of kelp.

One consequence of the weakening of tidal and wind-driven currents at both sites is that when mean currents are weak, wave-induced velocities become more important (Figures 3c and 4c). For example, at PP, in the absence of kelp (i.e., after September 2014), tidal velocities are comparable to or larger than wave-induced velocities, whereas, when kelp is present (i.e., July 2013 to September 2014), wave-induced velocities are dominant.

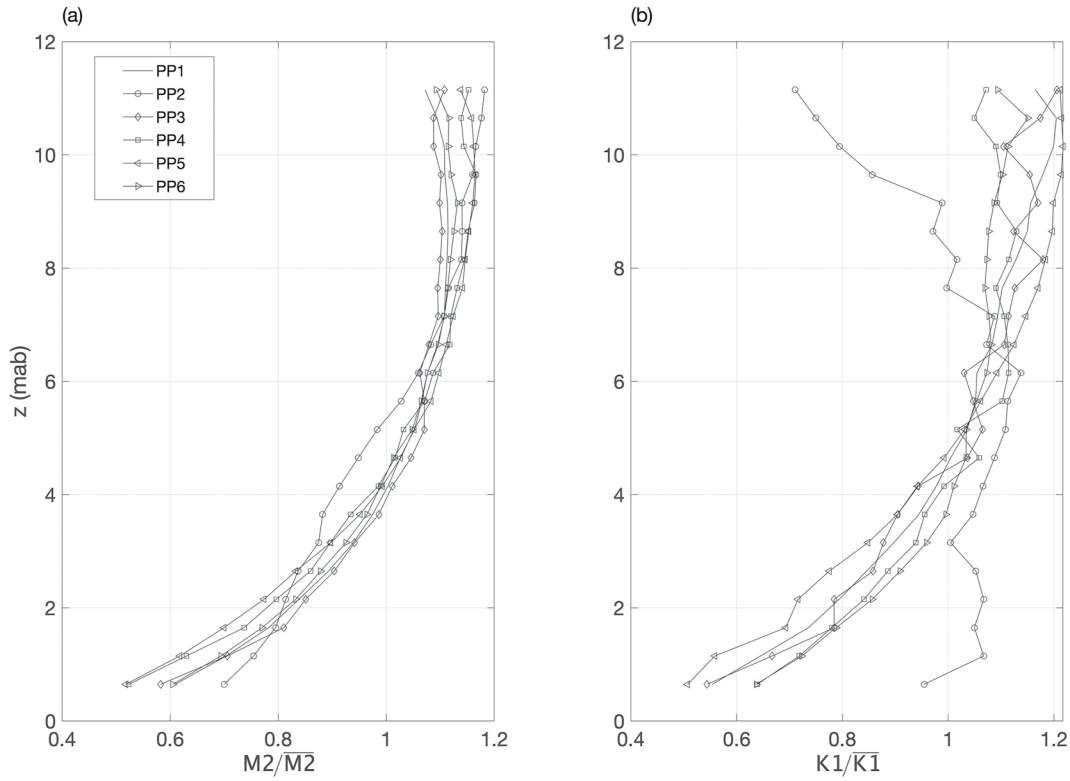

Figure 6. (a) M2 and (b) K1 amplitudes of longshore velocity at Punta Prieta as functions of height. Profiles for each period are scaled by their depth-averaged values. The legend in (a) shows which line corresponds to which deployment. Velocities used for scaling M2 amplitudes were: 0.14, 0.079, 0.060, 0.045, and 0.15 m/s. Velocities used for scaling K1 amplitudes were: 0.075, 0.022, 0.018, 0.013, 0.042, and 0.046 m/s.

Flows at MP behave in ways that are similar to what is seen at PP (Figure 4c), although flows at MP are much less tidally driven. Indeed, harmonic analysis of the MP data (Table S2 in Supporting Information S1) shows that while ~90% of the free-surface variance is due to tides, only ~30% of the velocity variance can be attributed to tides. Because of this, it is more challenging to quantify the effects of kelp biomass on flows at MP than PP, since at MP there is substantial variability associated with year-to-year differences in episodic wind events and upwelling strength that can mask the effects of kelp. In contrast, at PP, because tidal forcing is dominant, in effect, comparisons can be made between flows having the same forcing but different densities of kelp biomass. Consequently, much of the rest of the paper focuses on flows at PP, although, in order to illustrate the consistent effects of kelp, we will also show below several examples of flow behavior at MP.

The vertical structure of the tidal currents at PP is one feature of the flow that does not appear to vary with kelp biomass (Figure 6). When normalized by their depth averages (Table S1 in Supporting Information S1), and with one inexplicable exception, profiles of the M2 and K1 velocity constituents are remarkably constant, and similar in structure to each other. Because the ADP data do not extend through the upper 3 m of the water column, the velocity reduction due to the surface canopy measured in the laboratory by Rosman et al. (2010, 2013) may be only marginally apparent in the harmonic velocity profiles. Overall, the lack of a significant influence of kelp biomass on the vertical flow may reflect the position of the ADP in sand patches between nearby kelp stands. However, the distance between the kelp stands and the ADP would not seem to be sufficiently long for much modification of the velocity profile by turbulent mixing to have taken place.

In contrast, the vertical structure of the wind-driven flow at MP is different when kelp is present than when it is absent. As seen in Figure 7, a plot of the average current speed normalized by the near-bottom average speed, the flows are far more strongly sheared near the surface when the kelp canopy is absent then when the kelp canopy is present. Although analysis of this difference is beyond the scope of the present paper, it seems possible that this is a result of the high drag exerted by the surface canopy on the near-surface flow (Rosman et al., 2010).

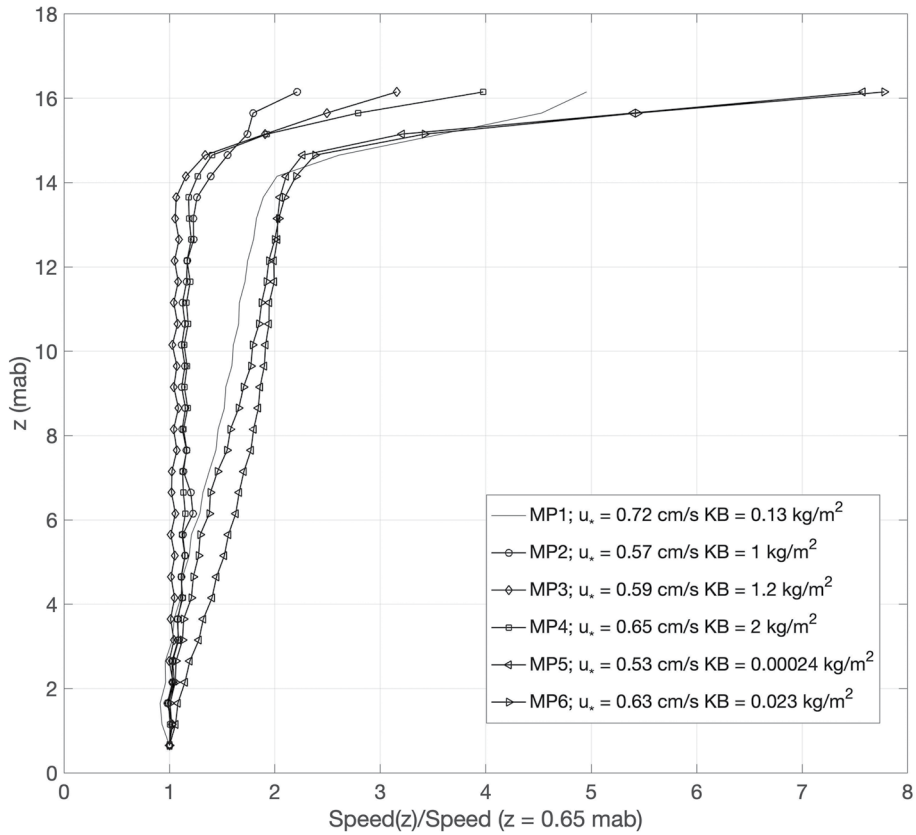

Figure 7. Vertical profiles of mean current speed at Morro Prieto. Each profile has been scaled by the mean velocity measured in the bin that was closest to the bottom (0.054, 0.046, 0.061, 0.046, 0.053, 0.052 m/s). Average wind stress shear velocity values for each deployment are also shown in the legend.

The effect of kelp on flow strength is best shown by the relationship between the depth-averaged alongshore velocity and kelp biomass, shown in Figure 8 as averages (denoted with angle brackets) of the absolute value of the velocity binned for different ranges of kelp biomass, normalized by the same average observed in the absence of kelp biomass:

$$V_r(KB_i) = \frac{\langle |V(KB_i)| \rangle}{\langle |V(KB_1)| \rangle} \quad KB_i \equiv KB \in [(i-1)\Delta KB, i\Delta KB] \quad \text{for } i = 1, 2, \ldots \tag{6}$$

Here, ΔKB is the width of the kelp biomass bins (0.1 kg/m^2), and the first bin, which has biomass KB_1, is defined as the no-kelp state. Figure 8 includes all the velocity data, with appropriate values of the satellite kelp biomass time series derived by linearly interpolating the kelp data onto the same time base as the velocity data. In terms of these ratios of averaged velocity, the effect of kelp seems to reach a maximum strength when kelp biomass is approximately 0.5 kg/m^2, with little effect beyond this value. The observed variation in V_r is due to the way drag is determined by the geometry of the kelp forest (Rosman et al., 2010, 2013), that is, the spatial density of kelp sporophytes (stipes, fronds, and canopy), a quantity that is proportional to kelp biomass density. An increase in kelp biomass means more drag elements per area and hence, for a given pressure gradient, reduced velocities. As seen in Figure 8, the currents at MP are reduced by a factor of 4 at high kelp biomass densities whereas at PP, the relative reduction is somewhat less, that is, by a factor of 2. It does not appear that this can be explained by the fact that peak biomass densities at MP are roughly 3 times those of PP, since the reduction in current strength at MP reaches a maximum at approximately the same kelp biomass density as is seen for the currents at PP.

A more nuanced view of how kelp affects flow can be had by comparing frequency spectra with and without kelp. To do this, consider spectra of longshore (v) and cross-shore (u) velocities for PP1 (no kelp) and PP4 (relatively high kelp). We have chosen these two deployments for comparison because they both span approximately

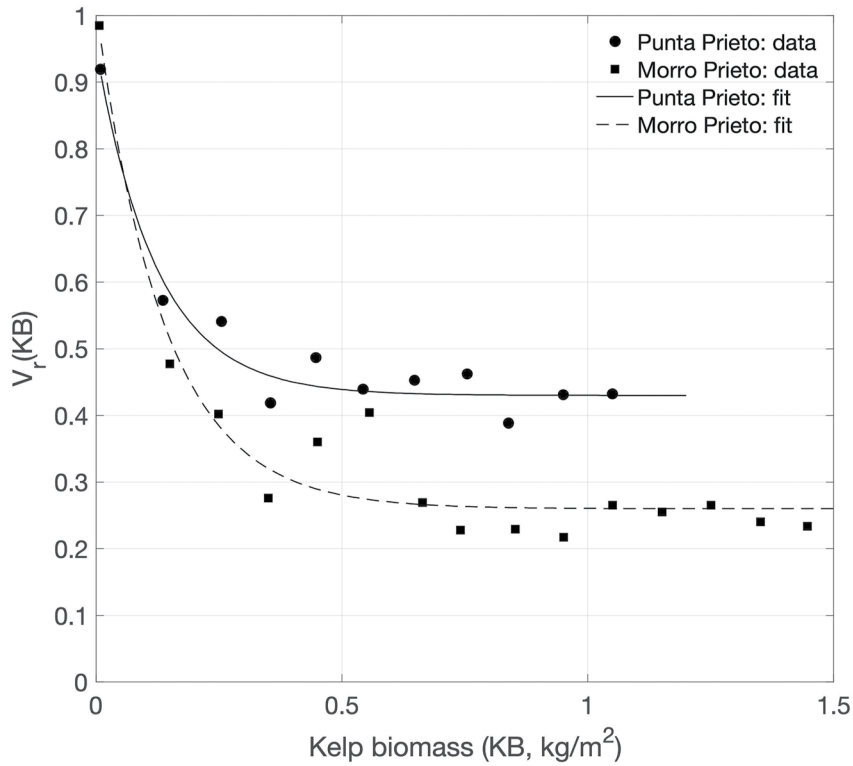

Figure 8. Ratios of mean absolute value of depth-averaged longshore velocity in the presence of kelp to its value in the absence of kelp, V_r. Data have been binned by kelp biomass so as to remove spring-neap and other longer period variability. Curve fits to data shown are for illustrative purposes only.

the same time of year. In both cases, alongshore velocity variances increase monotonically with height above bottom (Figures 9a and 9c), reflecting the structure of the primary tidal currents seen in Figure 7. The cross-shore flow in both cases is different: these flows are strongest near the surface and near the bottom. This suggests that the cross-shore flow is dominated by a vertically sheared exchange flow (see also Traiger et al. [2022]), one that varies at both diurnal and semi-diurnal frequencies.

One way to examine the frequency-dependent effect of kelp as a function of depth and frequency is to integrate the PSDs with respect to frequency separately for diurnal (0.7–1.4 cpd) and semidiurnal (1.7–2.3 cpd) frequency bands (Figure 10). This allows the frequency-dependent attenuation to be considered with more precision in that integration in frequency space removes some of the intrinsic variability associated with power spectral densities (PSD) estimation (Emery & Thomson, 2004). Remarkably, doing so shows that at diurnal frequencies, alongshore motions are ca. 5 ($\sqrt{20}$) times weaker when kelp is present than when kelp is absent, although the vertical structure of the flows is almost unchanged. Note that this attenuation is stronger than the factor of 2.7 that is inferred by considering the entire range of frequencies. Cross-shore flows are not as strongly affected by kelp: there is a factor of 1.4 difference between the two cases. For the semidiurnal frequency band, alongshore flows are reduced by a factor 2.6 and, as with the diurnal band, cross-shore flows are 1.4 times weaker.

The frequency-dependence of flow attenuation due to kelp can also be examined by first averaging the depth-dependent PSD given in Figure 9 over depth (Figures 11a and 11b) and then computing the frequency-dependent PSD ratios (Figures 11c and 11d). These PSD ratios show clearly that: (a) low frequencies are more strongly attenuated than high frequencies and (b) attenuation of cross-shore flows by kelp drag is weaker than is attenuation of alongshore flows.

Figure 12 shows the same quantities plotted in Figure 11 for the same time periods, but for the MP rather than PP data. Strikingly, the frequency dependence of the current attenuation seen in Figure 11 is the same as what is seen at MP, showing that the difference in current attenuation seen in Figure 8 are due to differences in the

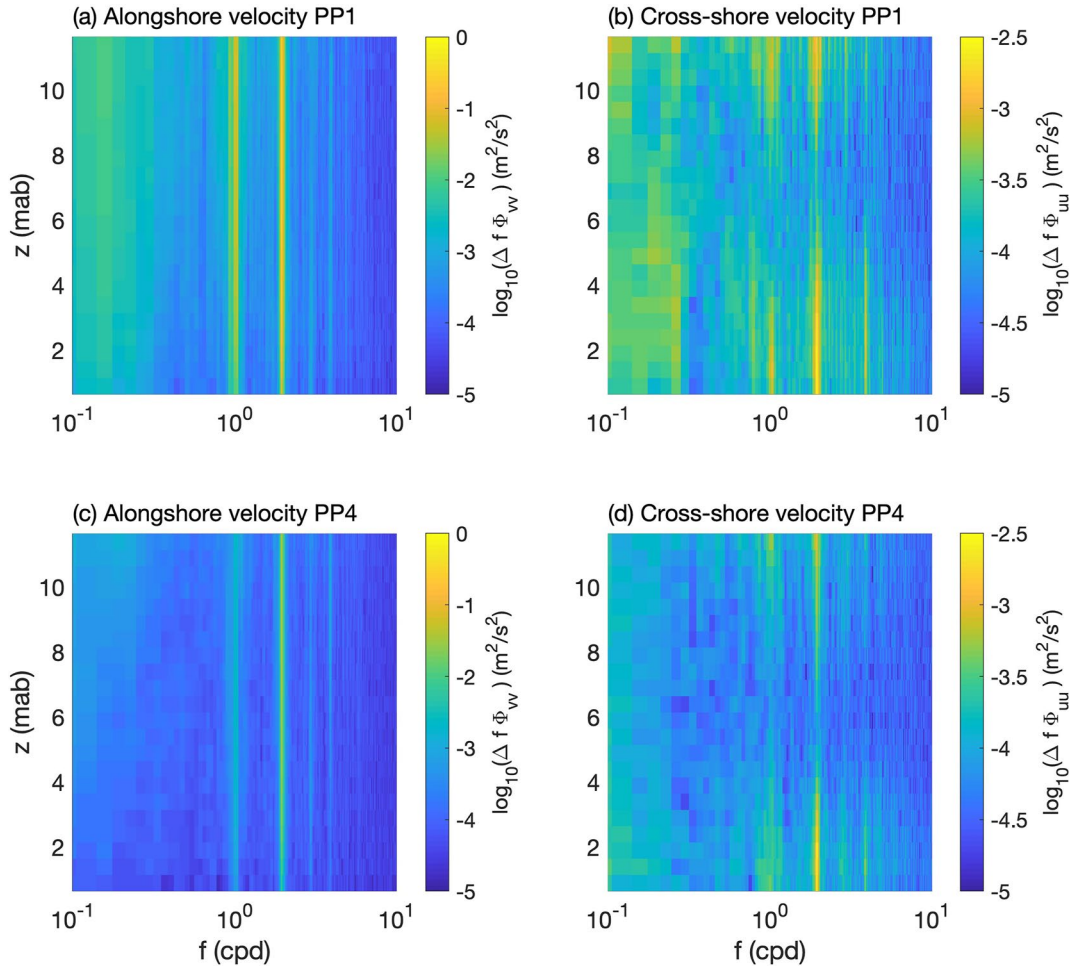

Figure 9. Power spectral densities as functions of frequency and depth at Punta Prieta for: (a) Longshore velocity during PP1 (KB = 3.8 g/m^2); (b) Cross-shore velocity during PP1; (c) Longshore velocity during PP4 (KB = 280 g/m^2); (d) Cross-shore velocity during PP4.

frequency dependence of the variance, with strongly attenuated subtidal frequencies being much more important at MP than at PP. Moreover, in light of Equations 2 and 3, the fact that frequency-dependent flow attenuation by kelp drag is the same at both sites, and that cross-shore flows are less attenuated than are longshore flows, supports the hypothesis that waves play relatively little role in creating drag on kelp since wave forcing at MP is generally larger than at PP (Figure S2 in Supporting Information S1). Indeed, this view is supported by Figure 3c, where little change in tidal currents at PP can be seen despite large changes in wave velocity. As suggested previously (Gaylord et al., 2008; Rosman et al., 2013; Utter & Denny, 1996), this may be due to the fact that the kelp sporophytes move with the waves, thus reducing the relative velocity between kelp and fluid that is responsible for drag creation.

4. Discussion

The influence of kelp presence or absence on flow speeds has been previously described (Gaylord et al., 2007; Jackson & Winant, 1983; Rosman et al., 2007). What is different in the present case is that we observed a direct effect on flow of kelp biomass, and were able to identify, for the first time, a biomass threshold beyond which additional biomass does not affect the flow. This was possible because the "natural" experiment of full deforestation caused by the combination of a prolonged warming event and storms allows for a comparison of flows before and after the loss of kelp. In all the other studies, the effect of kelp is estimated by comparing nearby locations inside and outside nearshore kelp forests. However, there are several factors that complicate this comparison: (a)

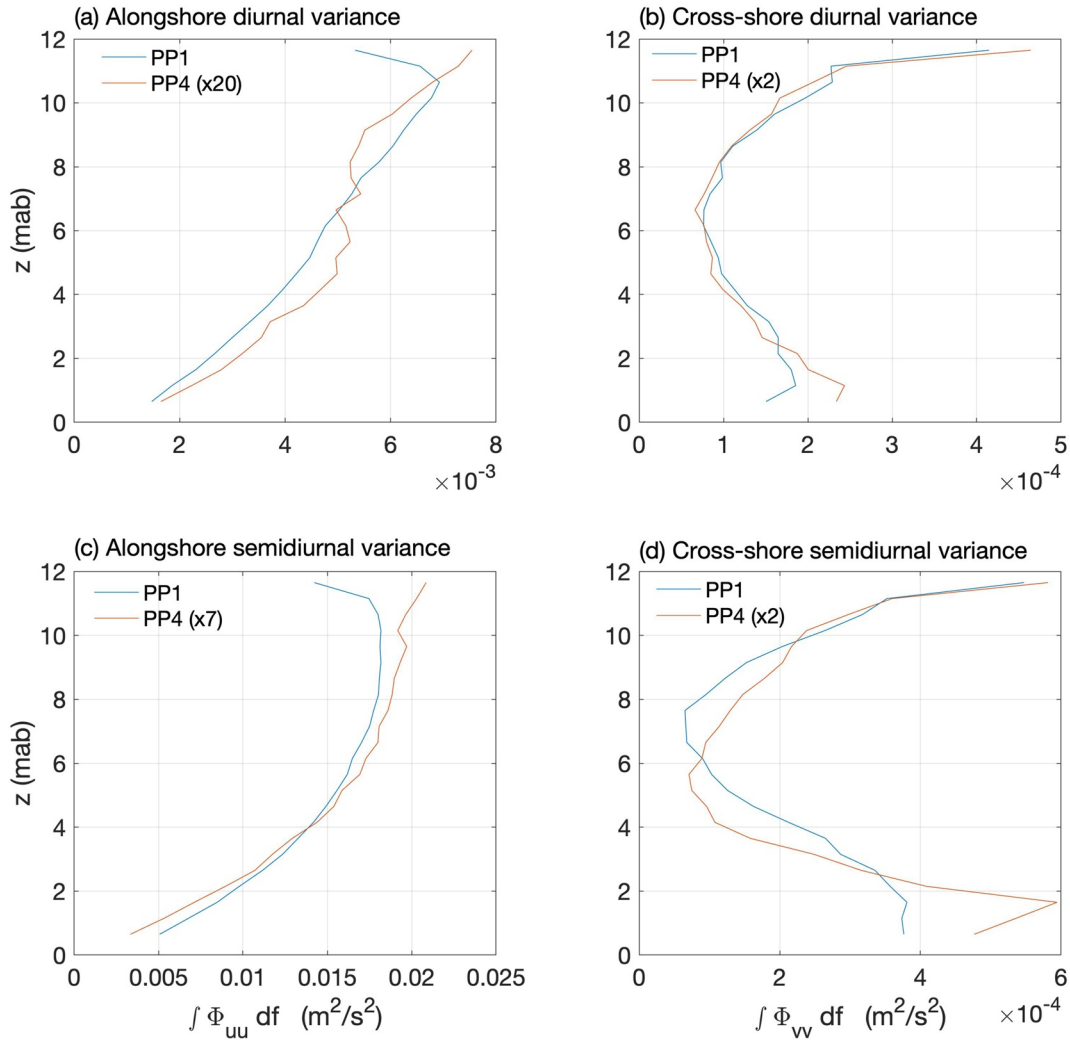

Figure 10. Vertical structure of the velocity variance in diurnal ($0.7 < f < 1.4$ cpd) and semi-diurnal frequency bands ($1.7 < f < 2.3$ cpd): (a) diurnal/longshore; (b) diurnal/cross-shore; (c) semidiurnal/longshore; and (d) semidiurnal/cross-shore. The gray shaded areas in Figures 11a–11d mark the two frequency bands plotted here.

Because the kelp forest partially blocks the flow locally, flows immediately outside are accelerated relative to further offshore, thus making the kelp effect appear stronger than it might be in reality depending on where the no kelp site is located (Gaylord et al., 2007); (b) In the presence of shoreline curvature, velocities can vary with cross-shore distance (Russell & Vennell, 2017); (c) Since depths inside the kelp forest and offshore will generally be different, the effects of waves on bottom stresses will be different. Thus, the present case is unique in that what we have observed are changes in flow due entirely to the presence or absence of kelp, controlling for all other factors.

The reductions in velocity due to kelp that we report here may be ecologically significant in several ways. First, flows determine the residence time, T_r, of anything, for example, particles or dissolved constituents like dissolved inorganic carbon (DIC), in the forest, since for flows at speed V through a kelp forest of length L, $T_r \sim L/V$. Assuming that the flux of the material of interest into or out of the flowing water, F, is independent of flow, then the change in concentration as water transits the kelp forest, $\Delta C \sim F\, T_r \sim F\, L/V$. Thus, for example, changes in DIC due to respiration and primary production (e.g., Frieder et al., 2012), will be inversely proportional to velocity and thus will be smaller in sparse kelp forests than in dense ones.

To allow for variations in time of V, T_r was computed using integration in time of the measured velocities as described above. Median values of T_r for alongshore and cross-shore flows near the surface ($z = 11.7$ mab) and

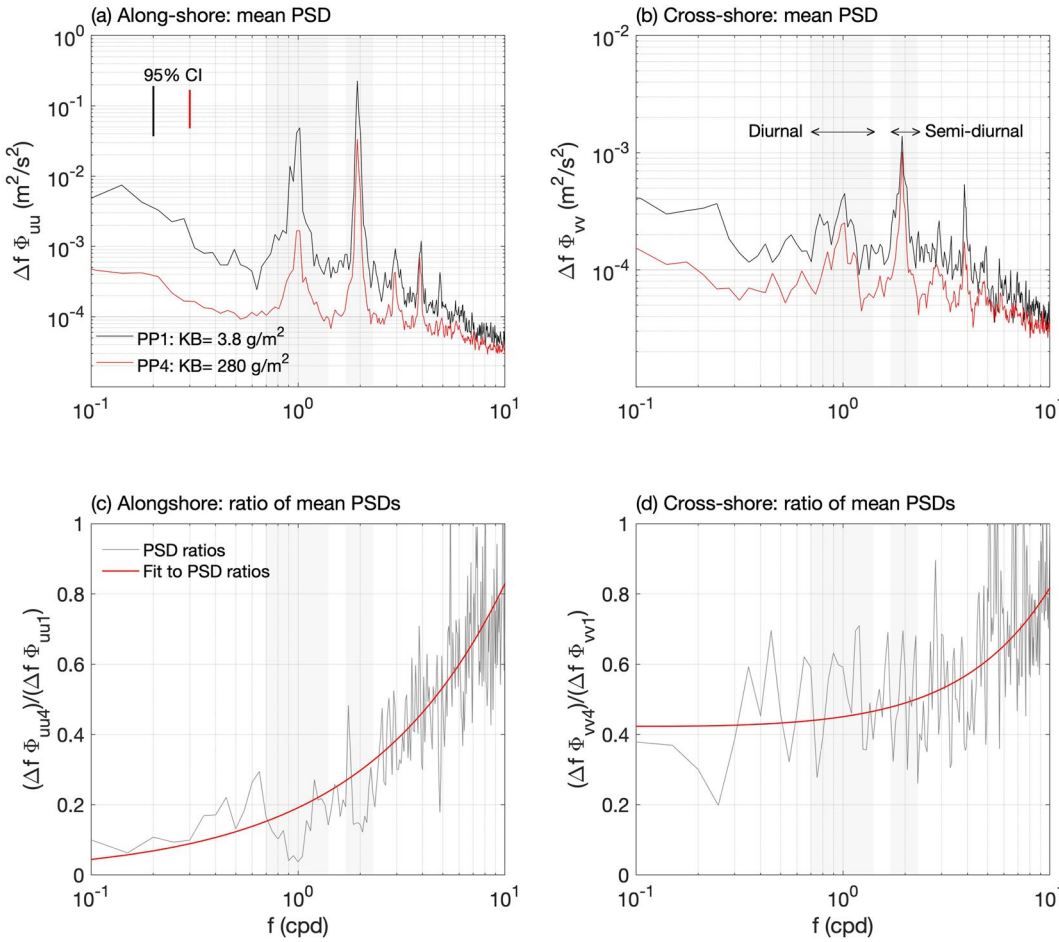

Figure 11. Depth-averaged power spectral densities as functions of frequency (*f*) at Punta Prieta for: (a) longshore velocities; and (b) cross-shore velocities. Ratios of power spectral densities for PP4 to those of PP1 for: (c) longshore velocities; and (d) cross-shore velocities. The legends in (a and c) also apply to (b and d). Confidence intervals for the spectra in (a and b) are shown in (a). The red lines in (c and d) show exponential fits to the power spectral density ratios. The gray bands in all panels show the approximate frequency ranges for diurnal and semidiurnal motions.

near the bottom ($z = 0.7$ mab), and for 5 of the 6 deployments, are given in Table 2. As would be expected given the vertical structure of the alongshore flow, residence times based on alongshore flows are shorter near the surface than near the bottom, and it is at the bottom where the effects of kelp on nominal retention are greatest. Despite the variability in T_r seen in the absence of kelp, it is clear that residence time based on alongshore flows increases substantially with increasing biomass, with near bottom values of T_r being as much as 10 times larger at a kelp biomass of ca. 300 g/m^2. However, residence times computed for cross-shore flows are somewhat shorter than for alongshore flows, that is, ca. 1 hr (median value) versus ca. 5 hr, implying that the principal means of exchange involve cross-shore flows. Surprisingly, these are not very different for the high and low kelp biomass cases, suggesting that residence time is little affected by the presence or absence of kelp.

While kelp biomass was highest during the third deployment, it is not included in Table 2 because computed residence times were close to those computed for times with no kelp. This may indicate that velocities measured by the ADP, located on the outer edge of the PP kelp forest, when the kelp forest had its highest biomass were not representative of velocities inside the kelp forest when the kelp forest had its highest biomass. Instead, the ADP measured flows reflecting the diversion of the oncoming flow around the kelp, as seen by Valle-Levinson et al. (2022). This would be consistent with the velocity measurements of Traiger et al. (2022), who observed near-zero alongshore velocities inside a kelp forest in Monterey Bay. Thus, in the case of high kelp biomass, T_r based on alongshore flows may become effectively infinite.

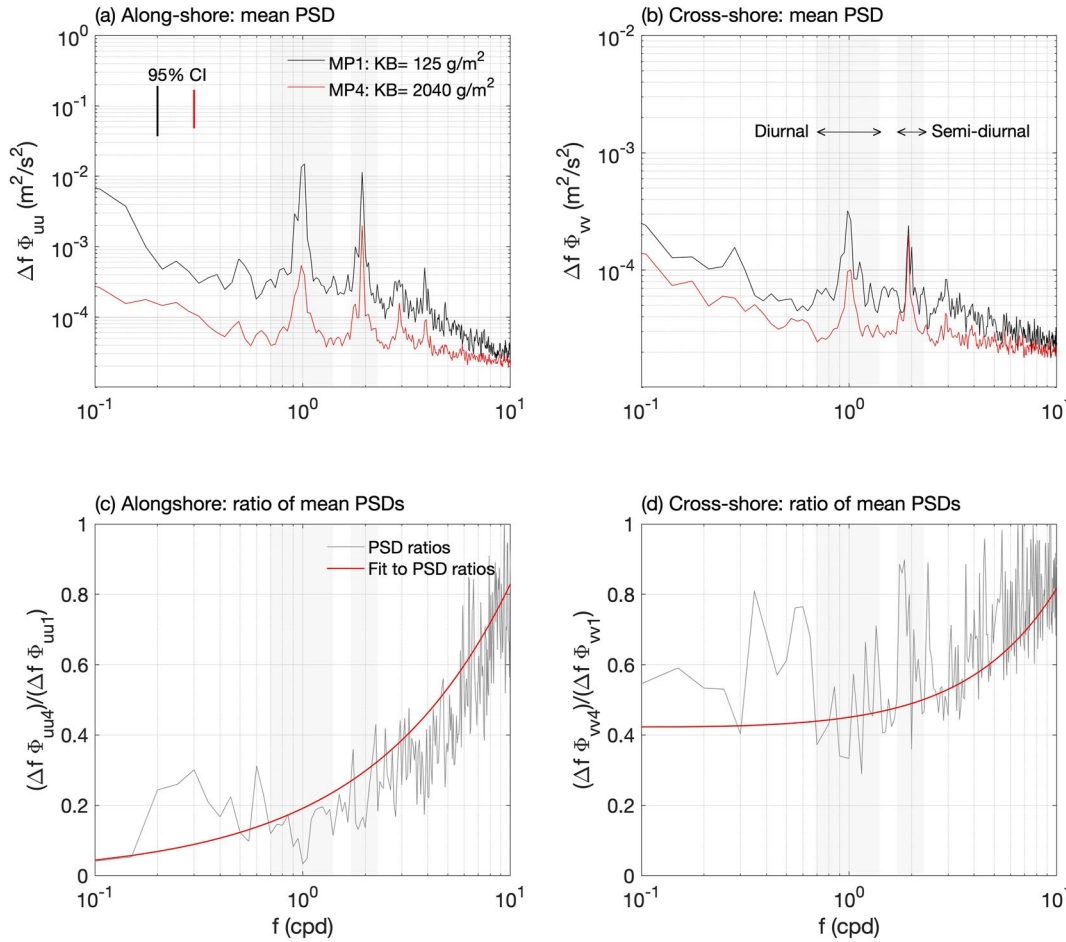

Figure 12. Depth-averaged power spectral densities as functions of frequency (f) at Morro Prieto. The plots shown here are otherwise the same as the ones in Figure 10. Note that the red lines in (c and d) show the *same* exponential fits to the power spectral density ratios shown in Figure 10.

Changes in velocities also imply changes in horizontal transport, represented here by tidal excursions, ζ (Equation 5), and thus of dispersal and recruitment of larvae, which in turn determine population connectivity, and therefore resilience to overexploitation and the optimal design of marine reserve networks (Cowen et al., 2007; Gaylord et al., 2012; Rossetto et al., 2015). Like velocities, ζ can also be cast in terms of its time-varying RMS value, ζ_{rms} (cf., Equation 4) which is close to being linearly proportional to V_{rms}. Thus, the observed factor of ~3 variation in V_{rms} (Figure 13b) due to kelp biomass variations translates into a factor of 3 variation in tidal excursion (Figure 13c). Thus, planktotrophic and lecitotrophic larvae would be transported farther alongshore, during their planktonic stages from where they are spawned in the absence of kelp than when kelp is present. Consequently, kelp presence may act to increase self-recruitment thus increasing larval spillover from marine reserves to local fishing grounds (e.g., Cudney-Bueno et al., 2009; Micheli et al., 2012) and the potential resilience of the abalone population following severe depletion (Smith et al., 2022). In contrast, the potential for long distance dispersal events increases dramatically when kelp is absent, providing a plausible mechanism for high regional connectivity and reducing the overall genetic structure of populations with limited larval durations and dispersal ability (Munguia-Vega et al., 2015).

Table 2
Calculated Median Residence Times at Punta Prieta

Period	*KB* (kg/m^2)	T_r (hr) alongshore near surface	T_r (hr) alongshore near bottom	T_r (hr) cross-shore near surface	T_r (hr) cross-shore near bottom
PP5	0	3.2	7.8	1.5	1.3
PP6	0	2.5	5	1.5	1.5
PP1	0.004	3.5	4.7	1.1	1.2
PP2	0.24	5.5	15	1.2	1.2
PP4	0.28	7.7	40	1.3	1.2

Second, the state of the kelp forest should also affect subtidal transport, although the exact extent is hard to determine because transport for scales

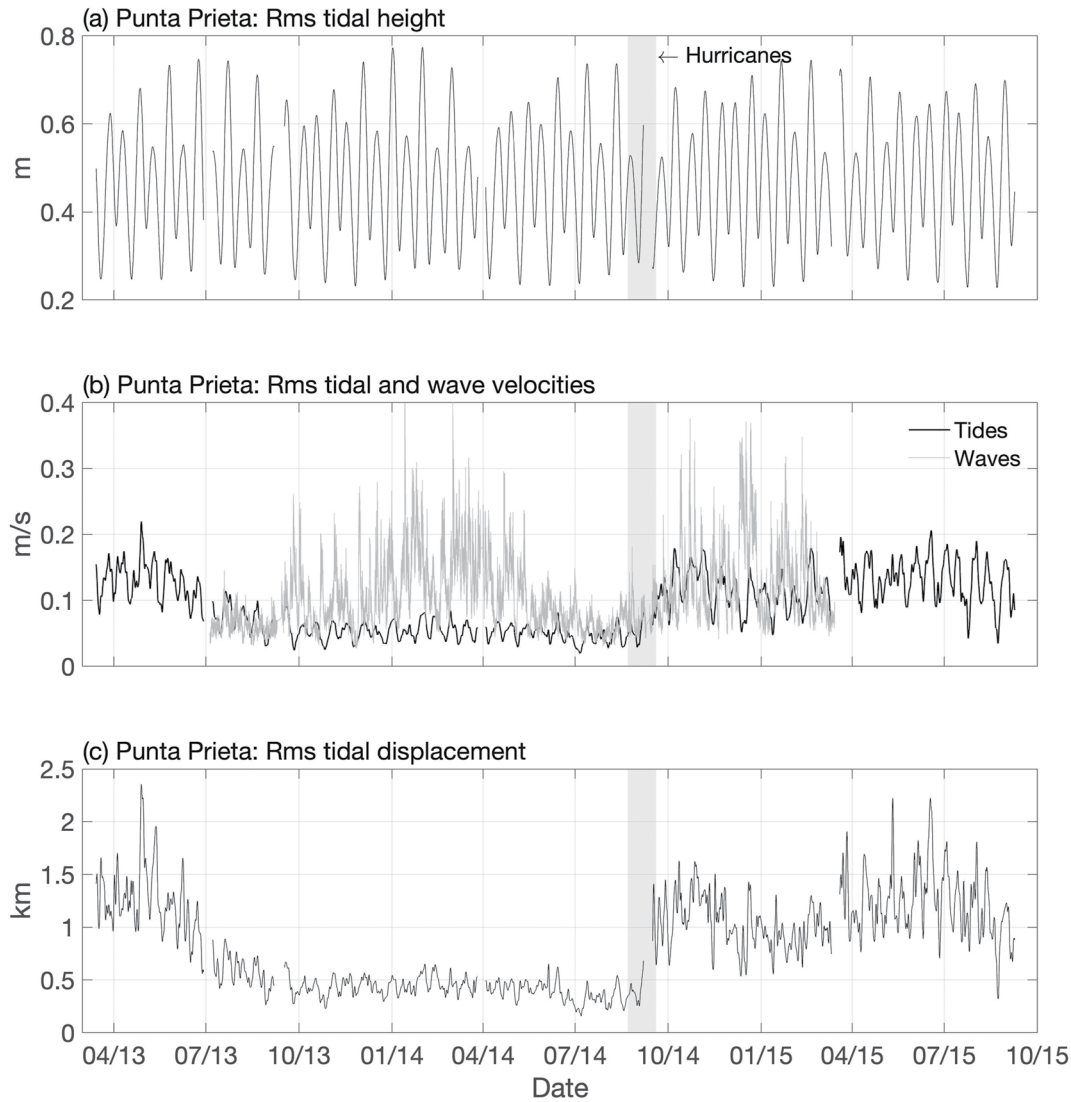

Figure 13. Variations at Punta Prieta in (a) tidal height H_{rms}; (b) root mean square (RMS) velocity for tides (–) and waves (–); and (c) RMS tidal displacement. The effects of the relatively high kelp biomass that existed between June 2013 and September 2014 can be clearly seen in (b and c) as reductions in velocities and thus displacements, although the tidal forcing (panel a) is the same for the other periods as it is for June 2013 to September 2014.

larger than the tidal excursion is likely controlled by the spatial variation in velocities, that is, progressive vector diagrams computed with velocities measured at single points are not likely to be reflective of transport at scales comparable to or larger than the length of the island. Indeed, even ζ and T_r as well (calculated as above) are only approximate. To properly represent water particle motions, the velocity used at each time step should be that appropriate to the particle's location at any time. Observationally, this would mean that either one deploys *many* instruments (as did Gaylord et al., 2007), or one should track Lagrangian particle displacements with neutrally buoyant drifters (e.g., Garwood et al., 2021). Nonetheless, we argue that our estimates of ζ and T_r based on data from a single ADP are sufficient to show the effects of the presence or absence of kelp.

This longer term transport behavior, no doubt affected by kelp forest state in ways that are similar to what we observe at tidal time scales, is likely important for management of the invertebrate fisheries because several of the targeted species, including abalone, sea cucumber, turban snail, and sea urchin, have short larval durations (3 days–4 weeks). For abalone, in particular, laboratory evaluation showed that larval development to settlement can take 3–10 days depending on temperature conditions (Leighton, 1974). Thus, the potential "seeding" effect of marine reserves, where populations protected in reserves replenish fished population through larval spillover,

for abalone and other harvested invertebrates, will be spatially dependent on the horizontal transport, and hence on the density of kelp biomass.

5. Conclusions

Our 2-1/2 year data set of nearshore flows through kelp forests on the shores of Isla Natividad allows us to unambiguously estimate the effect of kelp biomass on current strength. What is apparent from this comparison is that the effects of kelp are frequency dependent, as would be expected from the canopy flow literature and simple scaling (Lowe et al., 2005), with high-frequency motions damped less than low-frequency motions.

It is difficult to use the observations of current strength variations we present to construct predictive models of kelp drag that could be used in coastal circulation models. Indeed, we have avoided here the issue of using the data shown here to infer drag coefficients appropriate to depth-averaged flows (e.g., Lentz et al., 2017; Monismith et al., 2019). Monismith et al. (2022), develop and apply a simple theory for estimating drag from observations like those shown here. Unfortunately, this approach is largely empirical; that is, it does not provide a prediction of the relationship between flow and drag. This reflects two challenges: (a) the physics of drag on the kelp in the presence of waves and mean currents is remarkably complex (Gaylord et al., 2008, 2012; Rosman et al., 2013); (b) measuring kelp geometry, for example, number of stipes per holdfast or extent of the surface canopy, that is, the geometrical information needed to construct predictive models, is quite difficult. While satellite imagery has proven useful for monitoring large-scale changes in kelp forest condition (Bell et al., 2020), and aerial drones appear to offer a promising approach for detailed imaging of kelp forests (Cavanaugh et al., 2021), it is clear that more work is required to connect remote sensing products to the in-water surveys needed to accurately describe the details of kelp sporophyte geometry.

Finally, it is well known that large-scale interannual-to-interdecadal events can have large negative impacts on upwelling ecosystems and kelp forests, causing significant population redistribution and size reduction (Bell et al., 2020; Edwards, 2004; Hernandez-Carmona et al., 2000). The variation in kelp forest biomass around Isla Natividad observed throughout the study period is a particularly dramatic example of the changes in ecosystem structure that basin-scale oceanographic processes can induce. As we observed, physical changes in the kelp forests of Isla Natividad, with the significant warming of the Eastern Pacific in 2014–2015 altered flows in the nearshore regions important to abalone and other fisheries. These variations in flow with kelp biomass are important to managing and conserving kelp forest ecosystems and fisheries in the residence time of important biogeochemical conditions of the system, and connectivity, important to spatial dynamics of many kelp forest species, both are strongly affected by the physical state of the kelp forest. Thus, understanding the effects of the variation in kelp density on flow can inform the design and management of marine reserve networks, as well as the siting of artificial reefs, juvenile outplants, and other measures to protect and enhance fished populations. We can speculate that in a warming ocean, events like the 2014–2015 "deforestation" may become more common. Accordingly, ecosystem and/or population models and management strategies must recognize the important role played by biologically caused changes in hydrodynamics in shaping kelp forest ecosystems.

Acknowledgments
The work we describe here was supported by NSF grants DEB 1212124, OCE 1416934, OCE 1736830, and OCE 2022927, by an equipment grant from the Kuwait Foundation for the Advancement of Sciences, and through grants from the Marisla Foundation, Packard Foundation, and Walton Family Foundation. The authors are most grateful to the fishers and staff of the cooperative Buzos y Pescadores without whose remarkably generous assistance our project would have been impossible. The authors also wish to thank Justin Rogers, and Adam Greer, who helped with field work, and two anonymous reviewers whose comments improved the manuscript. Finally, the authors wish to thank Drs. Andrea Saenz-Arroyo and Jorge Torre, whose long-standing collaboration and guidance has played a key role in shaping our work at Isla Natividad.

Data Availability Statement

The processed data from the ADPs and thermistors as well as the time series of satellite estimated biomass discussed in this paper are available through the Stanford Digital Repository via the URL https://purl.stanford.edu/pm013yw3772 (https://doi.org/10.25740/pm013yw3772).

References

Alnajjar, M. W. (2019). *Nearshore processes of a coastal island: Physical dynamics and ecological implications* [PhD thesis]. Stanford University.

Arafeh-Dalmau, N., Schoeman, D., Montaño-Moctezuma, G., Micheli, F., Rogers-Bennett, L., Olguin-Jacobson, C., & Possingham, H. P. (2020). Marine heatwaves threaten kelp forests. *Science*, *367*, 635. https://doi.org/10.1126/science.aba5244

Arzeno, I. B., Collignon, A., Merrifield, M., Giddings, S. N., & Pawlak, G. (2018). An alongshore momentum budget over a fringing tropical fore-reef. *Journal of Geophysical Research: Oceans*, *123*, 7839–7855. https://doi.org/10.1029/2018JC014238

Bell, T. W., Allen, J. G., Cavanaugh, K. C., & Siegel, D. A. (2020). Three decades of variability in California's giant kelp forests from the Landsat satellites. *Remote Sensing of Environment*, *238*(1), 110811. https://doi.org/10.1016/j.rse.2018.06.039

Bell, T. W., Cavanaugh, K. C., & Siegel, D. A. (2015). Remote monitoring of giant kelp biomass and photosynthetic condition: An evaluation of the potential for the Hyperspectral Infrared Imager (HyspIRI) mission. *Remote Sensing of Environment*, *167*, 218–228. https://doi.org/10.1016/j.rse.2015.05.003

Bendat, J. S., & Piersol, A. G. (2000). *Random data analysis and measurement procedures* (3rd ed). Wiley-Interscience.

Cavanaugh, K. C., Cavanaugh, K. C., Bell, T. W., & Hockridge, E. G. (2021). An automated method for mapping giant kelp canopy dynamics from UAV. *Frontiers in Environmental Science*, *8*, 587354. https://doi.org/10.3389/fenvs.2020.587354

Cavanaugh, K. C., Reed, D. C., Bell, T. W., Castorani, M. C. N., & Beas-Luna, R. (2019). Spatial variability in the resistance and resilience of giant kelp in southern and Baja California to a multiyear heat wave. *Frontiers in Marine Science*, *6*, 413. https://doi.org/10.3389/fmars.2019.00413

Cavole, L. M., Demko, A. M., Diner, R. E., Giddings, A., Koester, I., Pagniello, C. M. L. S., et al. (2016). Biological impacts of the 2013–2015 warm-water anomaly in the Northeast Pacific: Winners, losers, and the future. *Oceanography*, *29*, 273–285. https://doi.org/10.5670/oceanog.2016.32

Cowen, R. K., Gawarkiewicz, G., Pineda, J., Thorrold, S. R., & Werner, F. E. (2007). Population connectivity in marine systems: An overview. *Oceanography*, *20*, 14–21. https://doi.org/10.5670/oceanog.2007.26

Cudney-Bueno, R., Lavin, M. F., Marinone, S. G., Raimondi, P. T., & Shaw, W. W. (2009). Rapid effects of marine reserves via larval dispersal. *PLoS One*, *4*, e4140. https://doi.org/10.1371/journal.pone.0004140

Dawson, E. Y. (1952). Circulation within Bahia Vizcaino, Baja California, and its effects on marine vegetation. *American Journal of Botany*, *39*, 425–432. https://doi.org/10.1002/j.1537-2197.1952.tb13050.x

Dean, R. G., & Dalrymple, R. A. (1991). *Water wave mechanics for engineers and scientists*. *Advanced Series on Ocean Engineering* (Vol. 2). World Scientific.

Edwards, M. S. (2004). Estimating scale-dependency in disturbance impacts: El Niños and giant kelp forests in the northeast Pacific. *Oecologia*, *138*, 436–447. https://doi.org/10.1007/s00442-003-1452-8

Elwany, M. H. S., O'Reilly, W. C., Guza, R. T., & Flick, R. E. (1995). Effects of Southern California kelp beds on waves. *Journal of Waterway, Port, Coastal, and Ocean Engineering*, *121*, 143–150. https://doi.org/10.1061/(ASCE)0733-950X(1995)121:2(143)

Emery, W. J., & Thomson, R. E. (2004). *Data analysis methods in physical oceanography* (2nd ed.). Elsevier.

Frieder, C. A., Nam, S. H., Martz, T. R., & Levin, L. A. (2012). High temporal and spatial variability of dissolved oxygen and pH in a nearshore California kelp forest. *Biogeosciences*, *9*, 917–3930. https://doi.org/10.5194/bg-9-3917-2012

Garwood, J. C., Lucas, A. J., Naughton, P., Roberts, P. L. D., Jaffe, J. S., de Gelleke, L., & Franks, P. J. S. (2021). Larval cross-shore transport estimated from internal waves with a background flow: The effects of larval vertical position and depth regulation. *Limnology & Oceanography*, *66*, 678–693. https://doi.org/10.1002/lno.11632

Gaylord, B., Denny, M. W., & Koehl, M. A. R. (2008). Flow forces on seaweeds: Field evidence for roles of wave impingement and organism inertia. *The Biological Bulletin*, *215*, 295–308. https://doi.org/10.2307/25470713

Gaylord, B., Nickols, K. J., & Jurgens, L. (2012). Roles of transport and mixing processes in kelp forest ecology. *Journal of Experimental Biology*, *215*, 997–1007. https://doi.org/10.1242/jeb.059824

Gaylord, B., Rosman, J. H., Reed, D. C., Koseff, J. R., Fram, J., MacIntyre, S., et al. (2007). Spatial patterns of flow and their modification within and around a giant kelp forest. *Limnology & Oceanography*, *52*, 1838–1852. https://doi.org/10.4319/lo.2007.52.5.1838

Godin, G. (1972). *The analysis of tides*. University of Toronto Press.

Hernandez-Carmona, G., Garcia, O., Robledo, D., & Foster, M. (2000). Restoration techniques for Macrocystis pyrifera (Phaeonphyceae) populations at the southern limit of their distribution in Mexico. *Botanica Marina*, *43*, 273–284.

Jackson, G. A., & Winant, C. D. (1983). Effect of a kelp forest on coastal currents. *Continental Shelf Research*, *2*, 75–80. https://doi.org/10.1016/0278-4343(83)90023-7

Leighton, D. L. (1974). The influence of temperature on larval and juvenile growth in three species of Southern California abalones. *Fishery Bulletin*, *72*, 1137–1145.

Lentz, S. J., Davis, K. A., Churchill, J. H., & DeCarlo, T. M. (2017). Coral reef drag coefficients–water depth dependence. *Journal of Physical Oceanography*, *47*(5), 1061–1075. https://doi.org/10.1175/jpo-d-16-0248.1

Lowe, R. J., Koseff, J. R., & Monismith, S. G. (2005). Oscillatory flow through submerged canopies. Part 1. Velocity structure. *Journal of Geophysical Research*, *110*, C10016. https://doi.org/10.1029/2004JC002788

Lucas, L. V., & Deleersnijder, E. (2020). Timescale methods for simplifying, understanding and modeling biophysical and water quality processes in coastal aquatic ecosystems: A review. *Water*, *12*, 2717. https://doi.org/10.3390/w12102717

McCay, B. J., Micheli, F., Ponce-Díaz, G., Murray, G., Shester, G., Ramirez-Sanchez, S., & Weisman, W. (2014). Cooperatives, concessions, and co-management on the Pacific coast of Mexico. *Marine Policy*, *44*, 49–59. https://doi.org/10.1016/j.marpol.2013.08.001

Micheli, F., Saenz-Arroyo, A., Greenley, A., Vazquez, L., Espinoza Montes, J. A., Rossetto, M., & De Leo, G. A. (2012). Evidence that marine reserves enhance resilience to climatic impacts. *PLoS One*, *7*, e40832. https://doi.org/10.1371/journal.pone.0040832

Monismith, S. G., Alnajjar, M., Daly, M., Valle-Levinson, A., Juarez, B., Fagundes, M., et al. (2022). Kelp forest drag coefficients derived from tidal flow data. *Estuaries and Coasts*.

Monismith, S. G., Hirsh, H., Batista, N., Francis, H., Egan, G., & Dunbar, R. B. (2019). Flow and drag in a seagrass bed. *Journal of Geophysical Research*, *124*, 2153–2163. https://doi.org/10.1029/2018JC0148622019

Munguia-Vega, A., Sáenz-Arroyo, A., Greenley, A. P., Espinoza Montes, J. A., Palumbi, S., Rossetto, M., & Micheli, F. (2015). Marine reserves help preserving genetic diversity after impacts derived from climate variability: Lessons from the pink abalone in Baja California. *Global Ecology and Conservation*, *4*, 264–276. https://doi.org/10.1016/j.gecco.2015.07.005

Nepf, H. M. (2012). Flow and transport in regions with aquatic vegetation. *Annual Review of Fluid Mechanics*, *44*, 123–142. https://doi.org/10.1146/annurev-fluid-120710-101048

Pawlowicz, R., Beardsley, B., & Lentz, S. (2002). Classical tidal harmonic analysis including error estimates in MATLAB using T_TIDE. *Computers & Geosciences*, *28*, 10–937. https://doi.org/10.1016/s0098-3004(02)00013-4

Reed, D., Washburn, L., Rassweiler, A., Miller, R., Bell, T., & Harrer, S. (2016). Extreme warming challenges sentinel status of kelp forests as indicators of climate change. *Nature Communications*, *7*(1), 13757. https://doi.org/10.1038/ncomms13757

Rominger, J. T., & Nepf, H. M. (2011). Flow adjustment and interior flow associated with a rectangular porous obstruction. *Journal of Fluid Mechanics*, *680*, 636–659. https://doi.org/10.1017/jfm.2011.199

Rosman, J. H., Denny, M. W., Zeller, R. B., Monismith, S. G., & Koseff, J. R. (2013). Interaction of waves and currents with kelp forests (*Macrocystis pyrifera*): Insights from a dynamically scaled laboratory model. *Limnology & Oceanography*, *58*, 790–802. https://doi.org/10.4319/lo.2013.58.3.0790

Rosman, J. H., Koseff, J. R., Monismith, S. G., & Grover, J. (2007). A field investigation into the effects of a kelp forest (Macrocystis pyrifera) on coastal hydrodynamics and transport. *Journal of Geophysical Research*, *112*, C02016. https://doi.org/10.1029/2005JC003430

Rosman, J. H., Monismith, S. G., Denny, M. A., & Koseff, J. R. (2010). Currents and turbulence within a kelp forest (Macrocystis pyrifera): Insights from a dynamically scaled laboratory model. *Limnology & Oceanography*, *55*, 1145–1158. https://doi.org/10.4319/lo.2010.55.3.1145

Rossetto, M., Micheli, F., Saenz-Arroyo, A., Espinoza Montes, J. A., & De Leo, G. A. (2015). No-take marine reserves can enhance population persistence and support the fishery of abalone. *Canadian Journal of Fisheries and Aquatic Science*, *72*, 1503–1517. https://doi.org/10.1139/cjfas-2013-0623

Russell, P., & Vennell, R. (2017). High-resolution observations of secondary circulation and tidally synchronized upwelling around a coastal headland. *Journal of Geophysical Research*, *122*, 890–913. https://doi.org/10.1002/2016JC012117

Smith, A., Aguilar, J. D., Boch, C. A., De Leo, G., Hernandez-Velasco, A., Houck, S., et al. (2022). Rapid recovery of depleted abalone in Isla Natividad, Baja California, Mexico. *Ecosphere*, *13*, e4002. https://doi.org/10.1002/ecs2.4002

Traiger, S. B., Cohn, B., Panos, D., Daly, M., Hirsh, H. K., Martone, M., et al. (2022). Biogeochemical modification of surface waters by kelp forest canopies: Influence of kelp metabolism and site-specific hydrodynamics. *Limnology & Oceanography*, *67*, 392–403. https://doi.org/10.1002/lno.11999

Utter, B. D., & Denny, M. W. (1996). Wave-induced forces on the giant kelp *Macrocystis pyrifera* (AGARDH): Field test of a computational model. *Journal of Experimental Biology*, *199*, 2645–2654. https://doi.org/10.1242/jeb.199.12.2645

Valle-Levinson, A., Daly, M. A., Juarez, B., Fagundes, M., Woodson, C. B., & Monismith, S. G. (2022). Influence of kelp forests on flow around headlands. *The Science of the Total Environment*, *825*, 153952. https://doi.org/10.1016/j.scitotenv.2022.153952

Walter, R. K., Woodson, C. B., Leary, P. R., & Monismith, S. G. (2014). Connecting regional dynamics and upwelling to nearshore internal bores and hypoxic events. *Journal of Geophysical Research: Oceans*, *119*(6), 3517–3534. https://doi.org/10.1002/2014JC009998

Wheeler, W. N. (1980). Effect of boundary layer transport on the fixation of carbon by the giant kelp *Macrocystis pyrifera*. *Marine Biology*, *56*, 103–110. https://doi.org/10.1007/bf00397128

Woodson, C. B., Micheli, F., Boch, C., Al-Najjar, M., Espinoza, A., Hernandez, A., et al. (2018). Harnessing marine microclimates for climate change adaptation and marine conservation. *Conservation Letts*, *12*, e12609. https://doi.org/10.1111/conl.12609